Isogeometric collocation methods for the Reissner-Mindlin plate problem

J. Kiendl [a,*], F. Auricchio [a,b], L. Beirão da Veiga [c], C. Lovadina [d,b], A. Reali [a,b]

[a] *Department of Civil Engineering and Architecture, University of Pavia*

[b] *IMATI–CNR, Pavia*

[c] *Mathematics Department "F.Enriques", University of Milan*

[d] *Mathematics Department, University of Pavia*

Abstract

Within the general framework of isogeometric methods, collocation schemes have been recently proposed as a viable and promising low-cost alternative to standard isogeometric Galerkin approaches. In this paper, isogeometric collocation methods for the numerical approximation of Reissner-Mindlin plate problems are proposed for the first time. Locking-free primal and mixed formulations are herein considered, and the potential of isogeometric collocation as a geometrically flexible and computationally efficient simulation tool for shear deformable plates is shown through the solution of several numerical tests.

Key words: Isogeometric analysis; collocation methods; NURBS; Reissner-Mindlin plate; locking-free methods.

1 Introduction

Isogeometric analysis (IGA) is a relatively new computational framework introduced by Hughes *et al.* [17,24] with the main goal of bridging the gap between Computer Aided Design (CAD) and Finite Element Analysis (FEA)

* Corresponding author.
Address: Department of Civil Engineering and Architecture, University of Pavia
Via Ferrata 3, 27100, Pavia, Italy
Phone: +39-0382-985016
E-mail: josef.kiendl@unipv.it

and of simplifying the expensive mesh generation process required by standard FEA. The basic IGA paradigm consists of adopting the same basis functions used for geometry representations in CAD systems - such as, e.g., Non-Uniform Rational B-Splines (NURBS) - for the approximation of field variables, in an isoparametric fashion. Thanks to the high-continuity properties of its basis functions, IGA is also characterized by an increased accuracy and robustness on a per-degree-of-freedom basis in comparison to standard FEA [8,10,18,25,30], and opens the door to new possibilities such as the construction of geometrically flexible discretizations of higher-order partial differential equations (PDEs) in primal form [2,21,28,31,35].

One of the main issues with IGA regards its efficient implementation and, in particular, the development of computationally efficient integration rules reducing assembly costs. In fact, in Galerkin IGA formulations, element-wise Gauss quadrature, typically adopted for standard FEA, is sub-optimal, since it does not take into account the inter-element higher continuity of the basis functions. More efficient quadrature rules have been developed by [6,26,34], but the development of a general and effective integration strategy for Galerkin isogeometric methods is still an open problem.

In an effort to minimize the computational cost, still preserving the advantages of IGA in terms of geometrical flexibility and accuracy, isogeometric collocation methods have been recently developed [3,4]. Isogeometric collocation is based on the discretization of the strong form of the governing PDEs within an isoparametric framework, taking advantage of the higher-continuity properties of the shape functions typically adopted in IGA. Isogeometric collocation has been proven to be an efficient tool able to attain high accuracy in combination with low computational costs, in particular when higher-order approximation degrees are adopted. An accurate comparison with (both IGA and FEA) Galerkin approaches has been carried out in [33].

In particular, isogeometric collocation looks extremely advantageous for explicit structural dynamics, where the computational cost is dominated by stress divergence evaluations at quadrature points for the calculation of the residual force vector [4], and, more in general, in all those situations where evaluation and assembly costs are dominant. In addition, it has been shown in [3] that, for a given bandwidth, IGA collocation typically achieves better convergence rates than IGA (or FEA) Galerkin. It should be however remarked that IGA collocation gives rise to non-symmetric (but diagonally dominant) stiffness matrices.

Within the isogeometric collocation context, several promising significant studies have been recently proposed, including phase-field modeling [22], contact [19], and hierarchical local refinement [33]. Among the many possible applications of IGA collocation, structural elements appear to be particularly in-

teresting. Within this framework, Bernoulli-Euler beam and Kirchhoff plate elements have been recently presented [32]. Also shear-deformable Timoshenko beams [12] and spatial rods [5] have been considered, using both primal and mixed formulations. Here, the peculiar structure of IGA collocation methods allows the construction of locking-free mixed methods independently of the approximation degrees for the three fields, and such a unique property has been proven analytically and extensively tested numerically.

Following the positive results obtained in the case of shear-deformable one-dimensional structures, in this paper, IGA collocation schemes are proposed for the first time for the numerical simulation of Reissner-Mindlin plate problems. We consider both primal and mixed formulations and show the potential of collocation methods to overcome shear locking within a geometrically flexible and computationally efficient framework. Several numerical tests are presented, proving the capabilities of the proposed formulations when different geometries and boundary conditions are considered.

The paper is organized as follows. In the second section, the PDEs governing the Reissner-Mindlin plate problem are introduced; both primal (i.e., based on displacements and rotations) and mixed (i.e., based on displacements, rotations, and shear forces) formulations are presented. In the third section, a brief introduction to B-Splines and NURBS is given, and the approximation of the geometry and of the field variables within the isogeometric analysis framework is presented. The fourth section is devoted to the description of the proposed collocation schemes for the approximation of the primal and mixed formulations previously considered. The fifth section is then devoted to numerical experiments showing the performance of the proposed methods, while, in the last section, conclusions and possible future research directions are drawn.

2 The Reissner-Mindlin plate problem

We consider a plate of constant thickness which is represented by its middle surface and the thickness t. The middle surface is comprised in the x-y-plane, while the z-direction is considered as the "thickness direction". The typical assumption for shear deformable plates is made, i.e., cross sections are assumed to remain straight during deformation but not necessarily normal to the middle surface. Also if unusual in finite element literature, in the following, the governing equations are not presented in matrix form but component-wise. This seems more appropriate for the collocation methods developed in this paper, since the final collocation equations are scalar equations associated to different sets of collocation points, as it will be discussed in detail below.

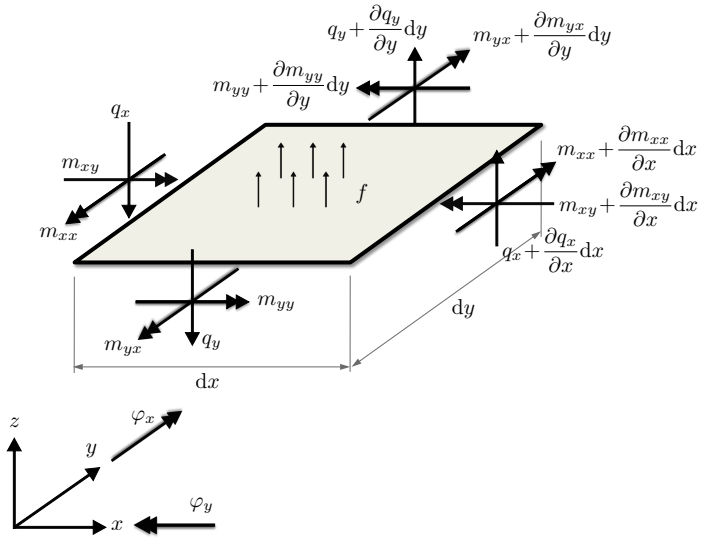

Fig. 1. Plate stress resultants and rotations.

2.1 Governing equations

The equilibrium equations are expressed in terms of stress resultants, in particular, the bending moments m_{xx}, m_{yy}, the twisting moments $m_{xy}=m_{yx}$, and the shear forces q_x, q_y. Figure 1 shows the stress resultants acting on an infinitesimal plate element $\mathrm{d}A=\mathrm{d}x\cdot\mathrm{d}y$ subjected to an external transversal load f. The plate equilibrium equations comprise the transversal equilibrium:

$$q_{x,x} + q_{y,y} = -f \tag{1}$$

and the rotational equilibrium in x and y:

$$m_{xx,x} + m_{xy,y} - q_x = 0 \tag{2}$$
$$m_{yy,y} + m_{yx,x} - q_y = 0 \tag{3}$$

Let w denote the transversal displacement, and let φ_x, φ_y denote the rotations of the plate cross section, with their orientation defined as depicted in Figure 1. Shear strains are denoted by γ_x and γ_y, with the same orientation definition as for the rotations. Then, the following kinematic equations hold:

$$w_{,x} = -\varphi_x + \gamma_x \tag{4}$$
$$w_{,y} = -\varphi_y + \gamma_y \tag{5}$$

Furthermore, we define the curvatures as the components of the symmetric

gradient of the rotations:

$$\kappa_{xx} = \varphi_{x,x} \tag{6}$$
$$\kappa_{yy} = \varphi_{y,y} \tag{7}$$
$$\kappa_{xy} = \kappa_{yx} = \frac{\varphi_{x,y} + \varphi_{y,x}}{2} \tag{8}$$

Assuming to deal with a linear elastic isotropic material and given the Young's modulus E, the Poisson's ratio ν, the shear modulus $G = E/(2+2\nu)$, and the plate thickness t, we define the plate bending stiffness parameter K_b and the shear stiffness parameter K_s as:

$$K_b = \frac{Et^3}{12(1-\nu^2)} \qquad K_s = \alpha\, Gt \tag{9}$$

The shear correction term α accounts for the non-constant distribution of shear stresses through the thickness. In the context of this paper, the standard value of $\alpha = 5/6$ is adopted.
According to the positions so far introduced, bending moments are related to the curvatures through the following relations:

$$m_{xx} = K_b(\kappa_{xx} + \nu\kappa_{yy}) \tag{10}$$
$$m_{yy} = K_b(\nu\kappa_{xx} + \kappa_{yy}) \tag{11}$$
$$m_{xy} = K_b(1-\nu)\,\kappa_{xy} \tag{12}$$

and shear forces are obtained from the shear strains by:

$$q_x = K_s\gamma_x \tag{13}$$
$$q_y = K_s\gamma_y \tag{14}$$

2.2 Possible problem formulations

We use the equilibrium, kinematic, and constitutive equations presented above in order to derive both a primal and a mixed formulation, which will be then used as basis for the collocation methods. For the primal formulation, we employ the standard approach of considering displacement and rotations as primal variables. An alternative approach could be to consider the displacement and the shear strains as primal variables, as shown in the context of Galerkin formulations in [11] for plates and in [20,29] for shells. For the mixed formulation, instead, shear forces are considered as independent variables additionally to displacement and rotations.

2.2.1 Primal formulation

Substituting the kinematic equations (4)-(8) into the constitutive equations (10)-(14), we can express bending moments and shear forces in terms of displacements and rotations:

$$m_{xx} = K_b(\varphi_{x,x} + \nu\varphi_{y,y}) \tag{15}$$
$$m_{yy} = K_b(\nu\varphi_{x,x} + \varphi_{y,y}) \tag{16}$$
$$m_{xy} = K_b\frac{1-\nu}{2}(\varphi_{x,y} + \varphi_{y,x}) \tag{17}$$

$$q_x = K_s(w_{,x} + \varphi_x) \tag{18}$$
$$q_y = K_s(w_{,y} + \varphi_y) \tag{19}$$

Substituting equations (15)-(19) into the equilibrium equations (1)-(3), we can express the equilibrium in terms of the primal variables:

$$K_s\ (w_{,xx} + w_{,yy} + \varphi_{x,x} + \varphi_{y,y}) = -f \tag{20}$$
$$K_s(-w_{,x} - \varphi_x) + K_b\left(\varphi_{x,xx} + \frac{1-\nu}{2}\varphi_{x,yy} + \frac{1+\nu}{2}\varphi_{y,xy}\right) = 0 \tag{21}$$
$$K_s(-w_{,y} - \varphi_y) + K_b\left(\varphi_{y,yy} + \frac{1-\nu}{2}\varphi_{y,xx} + \frac{1+\nu}{2}\varphi_{x,xy}\right) = 0 \tag{22}$$

Equations (20)-(22) represent the equilibrium equations in the interior of the domain while, at a Neumann boundary, the equilibrium is given by:

$$\mathbf{q}\cdot\mathbf{n} = \overline{q} \tag{23}$$
$$\mathbf{m}\cdot\mathbf{n} = \overline{\mathbf{m}} \tag{24}$$

where $\mathbf{q}$ is the vector of shear forces, $\mathbf{m}$ is the tensor of bending moments, $\mathbf{n} = [n_x, n_y]^{\mathrm{T}}$ is the outward normal vector to the boundary, $\overline{q}$ is a external shear force applied at the boundary, and $\overline{\mathbf{m}} = [\overline{m}_x, \overline{m}_y]^{\mathrm{T}}$ is the vector of external moments applied at the boundary.
Using equations (15)-(19), the boundary equilibrium equations (23)-(24) can be rewritten as follows:

$$K_s\left(n_x w_{,x} + n_y w_{,y} + n_x\varphi_x + n_y\varphi_y\right) = \overline{q} \tag{25}$$
$$K_b\left(n_x(\varphi_{x,x} + \nu\varphi_{y,y}) + n_y\frac{1-\nu}{2}(\varphi_{x,y} + \varphi_{y,x})\right) = \overline{m}_x \tag{26}$$
$$K_b\left(n_x\frac{1-\nu}{2}(\varphi_{x,y} + \varphi_{y,x}) + n_y(\nu\varphi_{x,x} + \varphi_{y,y})\right) = \overline{m}_y \tag{27}$$

Equations (20)-(22) and (25)-(27) are the equilibrium equations of the Reissner-Mindlin plate in a primal formulation in terms of displacement and rotations. These equations, together with the Dirichlet boundary conditions, are the basis for developing corresponding collocation methods as it will be shown in Section 4.1.

2.2.2 Mixed formulation

To establish a mixed formulation, we substitute again the kinematic (4)-(8) and the constitutive (10)-(14) equations into the equilibrium equations (1)-(3), but consider the shear forces q_x, q_y as additional independent variables:

$$q_{x,x} + q_{y,y} = -f \tag{28}$$

$$K_b \left(\varphi_{x,xx} + \frac{1-\nu}{2}\varphi_{x,yy} + \frac{1+\nu}{2}\varphi_{y,xy} \right) - q_x = 0 \tag{29}$$

$$K_b \left(\varphi_{y,yy} + \frac{1-\nu}{2}\varphi_{y,xx} + \frac{1+\nu}{2}\varphi_{x,xy} \right) - q_y = 0 \tag{30}$$

The relation between the shear forces and the primal variables is given by the constitutive equations (18)-(19):

$$K_s(w_{,x} + \varphi_x) - q_x = 0 \tag{31}$$

$$K_s(w_{,y} + \varphi_y) - q_y = 0 \tag{32}$$

Equations (28)-(32) represent a mixed formulation of the Reissner-Mindlin plate problem, being a system of five equations in five unknowns.
At Neumann boundaries, the equilibrium equations in the mixed formulation read as follows:

$$n_x q_x + n_y q_y = \overline{q} \tag{33}$$

$$K_b \left(n_x(\varphi_{x,x} + \nu\varphi_{y,y}) + n_y \frac{1-\nu}{2}(\varphi_{x,y} + \varphi_{y,x}) \right) = \overline{m}_x \tag{34}$$

$$K_b \left(n_x \frac{1-\nu}{2}(\varphi_{x,y} + \varphi_{y,x}) + n_y(\nu\varphi_{x,x} + \varphi_{y,y}) \right) = \overline{m}_y \tag{35}$$

The boundary equilibrium equations are complemented by the the constitutive equations (31)-(32), which hold equally in the interior of the domain and at the boundary. Equations (28)-(35), together with the Dirichlet boundary conditions, are the basis for developing a mixed collocation method as it will be shown in Section 4.2.

3 Isogeometric discretization with NURBS

For solving the equations presented in the previous section by isogeometric collocation, the unknown variables are discretized by Non-Uniform Rational B-Splines (NURBS).

3.1 B-splines and NURBS

B-splines are piecewise polynomials defined by the polynomial degree p and a so-called knot vector $[\xi_1, \xi_2, \ldots, \xi_{n+p+1}]$, where n is the number of basis functions. The knot vector is a set of parametric coordinates ξ_i, the so-called knots, which divide the parametric space into sections or knot spans. A knot can also appear repeatedly, in this case it is called a multiple knot. At a single knot the B-splines are C^{p-1} continuous, at a multiple knot of multiplicity k the continuity is reduced to C^{p-k}.

B-spline basis functions of degree p are defined by the following recursion formula. For $p = 0$:

$$N_{i,0}(\xi) = \begin{cases} 1, & \xi_i \leq \xi < \xi_{i+1} \\ 0, & \text{otherwise} \end{cases} \tag{36}$$

while for $p \geq 1$:

$$N_{i,p}(\xi) = \frac{\xi - \xi_i}{\xi_{i+p} - \xi_i} N_{i,p-1}(\xi) + \frac{\xi_{i+p+1} - \xi}{\xi_{i+p+1} - \xi_{i+1}} N_{i+1,p-1}(\xi) \tag{37}$$

A bivariate NURBS function R_{ij} is defined as the weighted tensor-product of the B-spline functions $N_{i,p}(\xi)$ and $M_{j,q}(\eta)$:

$$R_{ij}(\xi, \eta) = \frac{N_{i,p}(\xi) M_{j,q}(\eta) \omega_{ij}}{\sum_{k=1}^{n} \sum_{l=1}^{m} N_{k,p}(\xi) M_{l,q}(\eta) \omega_{kl}} \tag{38}$$

where ω_{ij} are called control weights. A NURBS surface $\mathbf{S}(\xi, \eta)$ is defined as a linear combination of basis functions and control points $\mathbf{P}_{ij}$:

$$\mathbf{S}(\xi, \eta) = \sum_{i=1}^{n} \sum_{j=1}^{m} R_{ij}(\xi, \eta) \mathbf{P}_{ij} \tag{39}$$

As in Galerkin-based isogeometric analysis, also in isogeometric collocation the isoparametric concept is adopted, i.e., NURBS are employed both to represent the geometry and to approximate the solution. Accordingly, the unknown

variables are approximated by:

$$w^h(\xi,\eta) = \sum_{i=1}^{n_w}\sum_{j=1}^{m_w} R_{ij}^{w}(\xi,\eta)\hat{w}^{ij} \tag{40}$$

$$\varphi_\xi^h(\xi,\eta) = \sum_{i=1}^{n_{\varphi\xi}}\sum_{j=1}^{m_{\varphi\xi}} R_{ij}^{\varphi_\xi}(\xi,\eta)\hat{\varphi}_\xi^{ij} \tag{41}$$

$$\varphi_\eta^h(\xi,\eta) = \sum_{i=1}^{n_{\varphi\eta}}\sum_{j=1}^{m_{\varphi\eta}} R_{ij}^{\varphi_\eta}(\xi,\eta)\hat{\varphi}_\eta{}^{ij} \tag{42}$$

$$q_\xi^h(\xi,\eta) = \sum_{i=1}^{n_{q\xi}}\sum_{j=1}^{m_{q\xi}} R_{ij}^{q_\xi}(\xi,\eta)\hat{q}_\xi{}^{ij} \tag{43}$$

$$q_\eta^h(\xi,\eta) = \sum_{i=1}^{n_{q\eta}}\sum_{j=1}^{m_{q\eta}} R_{ij}^{q_\eta}(\xi,\eta)\hat{q}_\eta{}^{ij} \tag{44}$$

As indicated in equations (40)-(44), different spaces can be employed for the discretization of the single fields. This fact is used, for instance, when creating the so-called rotated spaces for the rotations, as explained in the following section. We highlight that for the methods presented in this paper, different polynomial degrees might be used for the different fields, however, the same knot mesh is assumed for all discretized fields. Furthermore, continuity C^{p-1} is assumed for fields of order p, unless indicated otherwise.

3.2 Rotated spaces

A common problem of primal formulations in terms of displacement and rotations for Reissner-Mindlin plates is known as shear locking [7,13,23,27]. The problem typically appears for small values of the thickness parameter t and it is due to the fact that the spaces for displacement and rotations cannot represent the constraint of vanishing shear deformation, also known as the Kirchhoff constraint. In the thin limit ($t \to 0$), the shear strains must vanish and equations (4)-(5) reduce to:

$$\varphi_x = -w_{,x} \tag{45}$$

$$\varphi_y = -w_{,y} \tag{46}$$

In order to satisfy these equations in the discrete model, the spaces for φ_x^h and φ_y^h need to be chosen carefully. The isogeometric compatible spaces described below where introduced in [14,15] for electromagnetic problems, and first used in [9] for Reissner Mindlin plates with Galerkin IGA.

Let $S_{\alpha,\beta}^{p,q}$ denote the space of bivariate functions with polynomial degrees p, q and continuity indices α, β in ξ- and η-direction, respectively. We assume an

isotropic discretization, i.e., $p = q$ and $\alpha = \beta$, for the displacement:

$$w^h \in S^{p,p}_{\alpha,\alpha} \tag{47}$$

Accordingly, the spaces for the derivatives with respect to the parametric coordinates ξ, η are:

$$\frac{\partial w^h}{\partial \xi} \in S^{p-1,p}_{\alpha-1,\alpha} \tag{48}$$

$$\frac{\partial w^h}{\partial \eta} \in S^{p,p-1}_{\alpha,\alpha-1} \tag{49}$$

The derivatives with respect to the physical coordinates x, y are obtained from the derivatives with respect to the parametric coordinates ξ, η by the following mapping:

$$\begin{pmatrix} \dfrac{\partial w^h}{\partial x} \\ \dfrac{\partial w^h}{\partial y} \end{pmatrix} = \begin{pmatrix} \dfrac{\partial \xi}{\partial x} & \dfrac{\partial \eta}{\partial x} \\ \dfrac{\partial \xi}{\partial y} & \dfrac{\partial \eta}{\partial y} \end{pmatrix} \begin{pmatrix} \dfrac{\partial w^h}{\partial \xi} \\ \dfrac{\partial w^h}{\partial \eta} \end{pmatrix} \tag{50}$$

For a more compact notation in the following derivations, we use index notation ($x_1 = x, x_2 = y, \xi_1 = \xi, \xi_2 = \eta$) where the classical summation convention for repeated indices is used. Accordingly, equation (50) can be rewritten as:

$$\frac{\partial w^h}{\partial x_i} = \frac{\partial \xi_l}{\partial x_i} \frac{\partial w^h}{\partial \xi_l} \tag{51}$$

In order to have compatible spaces in equations (45)-(46), the spaces for the rotations φ_x and φ_y need to be chosen to according the gradient of the displacement, following the same steps as described in equations (48)-(51). First, the spaces for φ^h_ξ and φ^h_η are chosen according to the spaces of $w^h_{,\xi}$ and $w^h_{,\eta}$:

$$\varphi^h_\xi \in S^{p-1,p}_{\alpha-1,\alpha} \tag{52}$$

$$\varphi^h_\eta \in S^{p,p-1}_{\alpha,\alpha-1} \tag{53}$$

This is easily obtained due to the tensor product structure of the employed functions which allow choosing the polynomial degree and continuity independently for the two directions. Then, the rotation vector is mapped from the parametric space (φ^h_ξ, φ^h_η) to the physical space (φ_x, φ_y) by the same mapping as used for the gradient of the displacement described in (51):

$$\varphi^h_{x_i} = \frac{\partial \xi_l}{\partial x_i} \varphi^h_{\xi_l} \tag{54}$$

The first and second derivatives of the rotations in the physical space are then obtained as:

$$\frac{\partial \varphi^h_{x_i}}{\partial x_j} = \frac{\partial^2 \xi_l}{\partial x_i \partial x_j} \varphi^h_{\xi_l} + \frac{\partial \xi_l}{\partial x_i} \frac{\partial \varphi^h_{\xi_l}}{\partial x_j} \tag{55}$$

$$\frac{\partial \varphi^h_{x_i}}{\partial x_j \partial x_k} = \frac{\partial^3 \xi_l}{\partial x_i \partial x_j \partial x_k} \varphi^h_{\xi_l} + \frac{\partial^2 \xi_l}{\partial x_i \partial x_j} \frac{\partial \varphi^h_{\xi_l}}{\partial x_k} + \frac{\partial^2 \xi_l}{\partial x_i \partial x_k} \frac{\partial \varphi^h_{\xi_l}}{\partial x_j} + \frac{\partial \xi_l}{\partial x_i} \frac{\partial^2 \varphi^h_{\xi_l}}{\partial x_j \partial x_k} \tag{56}$$

Equations (54)-(56) represent the Piola mapping of the rotations and their derivatives, and the resulting spaces are referred to as rotated spaces. A discretization employing such spaces satisfies the compatibility conditions (52)-(53) and, as a consequence, is free of shear locking [9].

It is important to note that the rotated spaces (52)-(53) require the underlying spaces to be polynomial. This precludes the use of rational functions and B-Spline have to be used instead of NURBS to approximate the solution fields. As a consequence, the approach with rotated spaces is not isoparametric in a strict sense when the geometry is modeled by rational NURBS, as typically done for circular geometries. In Section 5.2 of this paper such an example is considered and successfully tested. The same approach has been employed in the context of an isogeometric Galerkin formulation for Reissner-Mindlin plates in [9] where the convergence of the approach is also proven analytically.

3.3 Boundary refinement

The Reissner-Mindlin plate problem can exhibit boundary layers [1], depending on the plate geometry, boundary conditions, and loading. Such boundary layers typically have a characteristic length $O(t)$. While their effects on the numerical solution are of minor importance for low-order finite elements, this is not the case for high-order and high-continuity isogeometric methods. As long as the mesh of the numerical model is not fine enough to properly resolve these layers, significant deterioration of convergence occurs [9]. Moreover, as shown in Section 5.3 of this paper, the use of a correct refinement in the presence of boundary layers seems even more important for collocation schemes than for Galerkin methods. In order to properly resolve the boundary layers but avoiding excessively fine meshes, the mesh refinement scheme needs to be adapted near the boundaries. In a NURBS-based model, this can be easily done by inserting additional knots near the boundary as shown in Section 5.2 of this paper. Within this study, we perform such refinement for problems where boundary layers are to be expected. Clearly, it would be interesting to develop an adaptive refinement algorithm which detects boundary layers and automatically performs problem-adapted mesh refinement, which, however, is beyond the scope of this work.

4 Collocation schemes

For the isogeometric collocation approach, the discretized strong form equations are collocated on the physical images of the Greville abscissae [3–5,12]. The Greville abscissae $\overline{\xi}$ related to a spline space of degree p and knot vector $\{\xi_1, \ldots, \xi_{n+p+1}\}$ are points of the parametric space defined by:

$$\overline{\xi}_i = \frac{\xi_{i+1} + \xi_{i+2} + \ldots + \xi_{i+p}}{p} \tag{57}$$

For two-dimensional problems, a Greville point is defined by $(\overline{\xi}, \overline{\eta})$, which are the Greville abscissae in the two parametric directions. For a shorter notation, we write $\overline{\boldsymbol{\xi}} = (\overline{\xi}, \overline{\eta})$. It should be noted that according to equation (57), the first and the last Greville abscissae are located at the boundaries. Since the equilibrium equations to be collocated are different at the boundary and the domain interior, we introduce the following notation for different sets of Greville points: $\{\overline{\boldsymbol{\xi}}\}$ denotes the set of all Greville points of the associated space, i.e., $\{\overline{\boldsymbol{\xi}}\} = \overline{\boldsymbol{\xi}}_{ij} (i = 1 \ldots n, \quad j = 1 \ldots m)$, while $\{\overline{\boldsymbol{\xi}}\}^{\Omega}$ denotes the set of the Greville points excluding the boundaries, i.e., $\{\overline{\boldsymbol{\xi}}\}^{\Omega} = \overline{\boldsymbol{\xi}}_{ij} (i = 2 \ldots n\text{–}1, \quad j = 2 \ldots m\text{–}1)$ and $\{\overline{\boldsymbol{\xi}}\}^{\Gamma}$ denotes the Greville points on the boundaries, i.e., $\{\overline{\boldsymbol{\xi}}\}^{\Gamma} = \{\overline{\boldsymbol{\xi}}\} \backslash \{\overline{\boldsymbol{\xi}}\}^{\Omega}$. If rotated spaces are used as described above, different sets of Greville points are obtained for the different fields. For a clear distinction, these are denoted by $\overline{\boldsymbol{\xi}}_w$, $\overline{\boldsymbol{\xi}}_{\varphi_\xi}$, and $\overline{\boldsymbol{\xi}}_{\varphi_\eta}$ referring to the different spaces of displacement and rotations. Finally, the physical image of a Greville point is obtained by the NURBS mapping $\mathbf{S}(\overline{\boldsymbol{\xi}})$.

4.1 Primal formulation

In the following, we develop two collocation schemes based on the primal formulation, one using equal orders for the different fields and one using rotated spaces. For this purpose, we discretize the equilibrium equations (20)-(27) and write them in a residual form, i.e., $R = 0$, with R being the residual. In particular, we define the residual of the transversal equilibrium equation on the domain interior (20):

$$R_w^{\Omega} = K_s (w^h_{,xx} + w^h_{,yy} + \varphi^h_{x,x} + \varphi^h_{y,y}) + f \tag{58}$$

Similarly, we define the residual of the interior domain equation of rotational equilibrium in x (21):

$$R_{\varphi_x}^{\Omega} = K_s (-w^h_{,x} - \varphi^h_x) + K_b \left(\varphi^h_{x,xx} + \frac{1-\nu}{2} \varphi^h_{x,yy} + \frac{1+\nu}{2} \varphi^h_{y,xy} \right) \tag{59}$$

and of rotational equilibrium in y (22):

$$R^{\Omega}_{\varphi_y} = K_s(-w^h_{,y} - \varphi^h_y) + K_b\left(\varphi^h_{y,yy} + \frac{1-\nu}{2}\varphi^h_{y,xx} + \frac{1+\nu}{2}\varphi^h_{x,xy}\right) \tag{60}$$

In an analogous manner, we define the residuals corresponding to the equilibrium equations at the boundary (25)-(27):

$$R^{\Gamma}_{w} = K_s\left(n_x w^h_{,x} + n_y w^h_{,y} + n_x\varphi^h_x + n_y\varphi^h_y\right) - \overline{q} \tag{61}$$

$$R^{\Gamma}_{\varphi_x} = K_b\left(n_x(\varphi^h_{x,x} + \nu\varphi^h_{y,y}) + n_y\frac{1-\nu}{2}(\varphi^h_{x,y} + \varphi^h_{y,x})\right) - \overline{m}_x \tag{62}$$

$$R^{\Gamma}_{\varphi_y} = K_b\left(n_x\frac{1-\nu}{2}(\varphi^h_{x,y} + \varphi^h_{y,x}) + n_y(\nu\varphi^h_{x,x} + \varphi^h_{y,y})\right) - \overline{m}_y \tag{63}$$

4.1.1 Primal formulation with equal orders

For the collocation scheme with equal orders, i.e., all the discrete spaces in (40)-(42) using the same knot vector and polynomial order, there is one unique set of Greville points, which is used to collocate the equilibrium equations as given in (58)-(63). In particular, equations (58)-(60) are collocated on the domain interior, while equations (61)-(63) are collocated on Neumann boundaries [1] . Accordingly, we propose the following collocation scheme.

Collocate :

$$R^{\Omega}_{w} = 0, \quad R^{\Omega}_{\varphi_x} = 0, \quad R^{\Omega}_{\varphi_y} = 0 \quad \text{on} \quad \mathbf{S}(\{\overline{\boldsymbol{\xi}}\}^{\Omega}) \tag{64}$$

$$R^{\Gamma}_{w} = 0, \quad R^{\Gamma}_{\varphi_x} = 0, \quad R^{\Gamma}_{\varphi_y} = 0 \quad \text{on} \quad \mathbf{S}(\{\overline{\boldsymbol{\xi}}\}^{\Gamma}) \tag{65}$$

The equations above describe a free plate, i.e. with full Neumann boundaries. For clamped or supported boundaries, the associated Dirichlet conditions are directly applied to the respective degrees of freedom and substituted to the related equation in (65).

4.1.2 Primal formulation with rotated spaces

In a primal formulation with rotated spaces, different NURBS spaces are used for the three fields $w, \varphi_\xi, \varphi_\eta$, and, accordingly, there are three different sets

[1] Here and in the following, we choose to directly collocate Neumann boundary conditions on Neumann boundaries in agreement with what has been typically done in the IGA collocation literature. However, we remark that it has been recently shown in [19] that such an approach may not be optimal in singular situations, in particular when non-uniform meshes are adopted. To properly deal with those situations, simple alternative strategies have been therein proposed, and could be verbatim adopted also in the context of this paper.

of collocation points. Inspired by the variational formulation of the problem, we propose to collocate the equation of transversal equilibrium on the Greville points related to the displacement space, and the equations of rotational equilibrium on the Greville points related to the respective rotation spaces. It is important to note that the residuals given in (59)-(60) and (62)-(63) refer to the equilibrium of rotations in x and y, i.e., to φ_x and φ_y. The collocation points, however, are defined by the Greville abscissae of the spaces for φ_ξ and φ_η. Consequently, the equations of rotational equilibrium must be formulated in terms of $\varphi_\xi, \varphi_\eta$, which is obtained by the following transformation of the residuals:

$$\begin{pmatrix} R_{\varphi_\xi} \\ \\ R_{\varphi_\eta} \end{pmatrix} = \begin{pmatrix} \dfrac{\partial \xi}{\partial x} & \dfrac{\partial \xi}{\partial y} \\ \dfrac{\partial \eta}{\partial x} & \dfrac{\partial \eta}{\partial y} \end{pmatrix} \begin{pmatrix} R_{\varphi_x} \\ \\ R_{\varphi_y} \end{pmatrix} \tag{66}$$

This transformations is applied to the residuals of rotational equilibrium both on the domain interior (59)-(60) and at the boundary (62)-(63).
Accordingly, the following collocation scheme is proposed for the primal formulation with rotated spaces:

$$\begin{aligned} &\textit{Collocate}: \\ &R_w^\Omega = 0 \quad \text{on} \quad \mathbf{S}(\{\overline{\boldsymbol{\xi}}_w\}^\Omega) && (67)\\ &R_{\varphi_\xi}^\Omega = 0 \quad \text{on} \quad \mathbf{S}(\{\overline{\boldsymbol{\xi}}_{\varphi_\xi}\}^\Omega) && (68)\\ &R_{\varphi_\eta}^\Omega = 0 \quad \text{on} \quad \mathbf{S}(\{\overline{\boldsymbol{\xi}}_{\varphi_\eta}\}^\Omega) && (69)\\ &R_w^\Gamma = 0 \quad \text{on} \quad \mathbf{S}(\{\overline{\boldsymbol{\xi}}_w\}^\Gamma) && (70)\\ &R_{\varphi_\xi}^\Gamma = 0 \quad \text{on} \quad \mathbf{S}(\{\overline{\boldsymbol{\xi}}_{\varphi_\xi}\}^\Gamma) && (71)\\ &R_{\varphi_\eta}^\Gamma = 0 \quad \text{on} \quad \mathbf{S}(\{\overline{\boldsymbol{\xi}}_{\varphi_\eta}\}^\Gamma) && (72) \end{aligned}$$

The same observations of Section 4.1.1 regarding Neumann and Dirichlet boundary conditions apply in this case.

4.2 Mixed formulation with equal orders

For the mixed formulation, equal orders are used for all variables in (40)-(44). Accordingly, there is a unique set of Greville points as basis to collocate the corresponding equations (28)-(35). Nevertheless, it must be distinguished between equations to be collocated on the domain interior, at the boundary, or on the whole domain.
Accordingly, we propose the following collocation scheme for the mixed for-

mulation:

$$q^h_{x,x} + q^h_{y,y} + f = 0 \quad \text{on } \mathbf{S}(\{\overline{\boldsymbol{\xi}}\}^{\Omega}) \tag{73}$$

$$K_b\left(\varphi^h_{x,xx} + \frac{1-\nu}{2}\varphi^h_{x,yy} + \frac{1+\nu}{2}\varphi^h_{y,xy}\right) - q^h_x = 0 \quad \text{on } \mathbf{S}(\{\overline{\boldsymbol{\xi}}\}^{\Omega}) \tag{74}$$

$$K_b\left(\varphi^h_{y,yy} + \frac{1-\nu}{2}\varphi^h_{y,xx} + \frac{1+\nu}{2}\varphi^h_{x,xy}\right) - q^h_y = 0 \quad \text{on } \mathbf{S}(\{\overline{\boldsymbol{\xi}}\}^{\Omega}) \tag{75}$$

$$n_x q^h_x + n_y q^h_y - \overline{q} = 0 \quad \text{on } \mathbf{S}(\{\overline{\boldsymbol{\xi}}\}^{\Gamma}) \tag{76}$$

$$K_b\left(n_x(\varphi^h_{x,x} + \nu\varphi^h_{y,y}) + n_y\frac{1-\nu}{2}(\varphi^h_{x,y} + \varphi^h_{y,x})\right) - \overline{m}_x = 0 \quad \text{on } \mathbf{S}(\{\overline{\boldsymbol{\xi}}\}^{\Gamma}) \tag{77}$$

$$K_b\left(n_x\frac{1-\nu}{2}(\varphi^h_{x,y} + \varphi^h_{y,x}) + n_y(\nu\varphi^h_{x,x} + \varphi^h_{y,y})\right) - \overline{m}_y = 0 \quad \text{on } \mathbf{S}(\{\overline{\boldsymbol{\xi}}\}^{\Gamma}) \tag{78}$$

$$K_s\left(w^h_{,x} + \varphi^h_x\right) - q^h_x = 0 \quad \text{on } \mathbf{S}(\{\overline{\boldsymbol{\xi}}\}) \tag{79}$$

$$K_s\left(w^h_{,y} + \varphi^h_y\right) - q^h_y = 0 \quad \text{on } \mathbf{S}(\{\overline{\boldsymbol{\xi}}\}) \tag{80}$$

where equations (73)-(75) represent the equilibrium equations on the domain interior, (76)-(78) the equilibrium equations on the Neumann boundaries, and (79)-(80) are the constitutive equations valid on the whole domain including the boundaries. As in the primal formulations, Dirichlet boundary conditions are directly applied to the respective degrees of freedom.

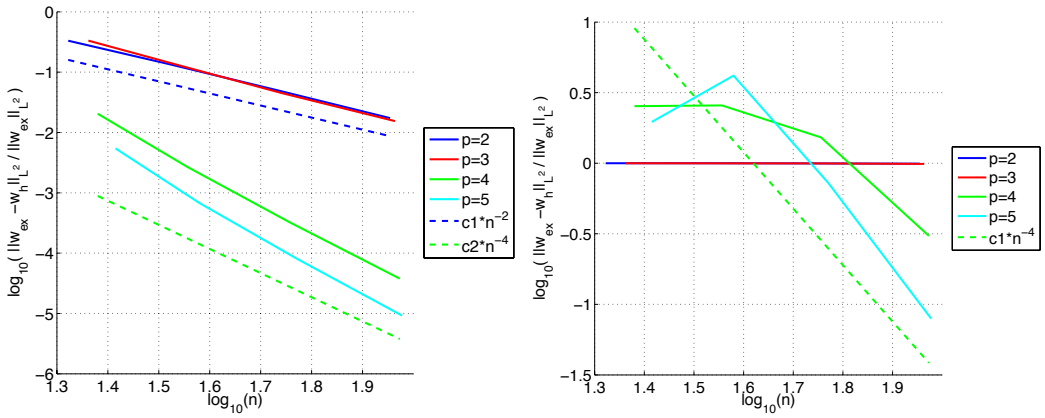

(a) $t = 10^{-1}$ (b) $t = 10^{-3}$

Fig. 2. Square plate with clamped support solved by a *primal formulation with equal orders*. L^2-norm approximation error of *displacement* for (a) a thick plate and (b) a thin plate.

5 Numerical tests

In this section, we perform numerical convergence analysis of the proposed methods using two different test examples. The first example consists of a simple square plate with clamped supports having a known analytical solution.

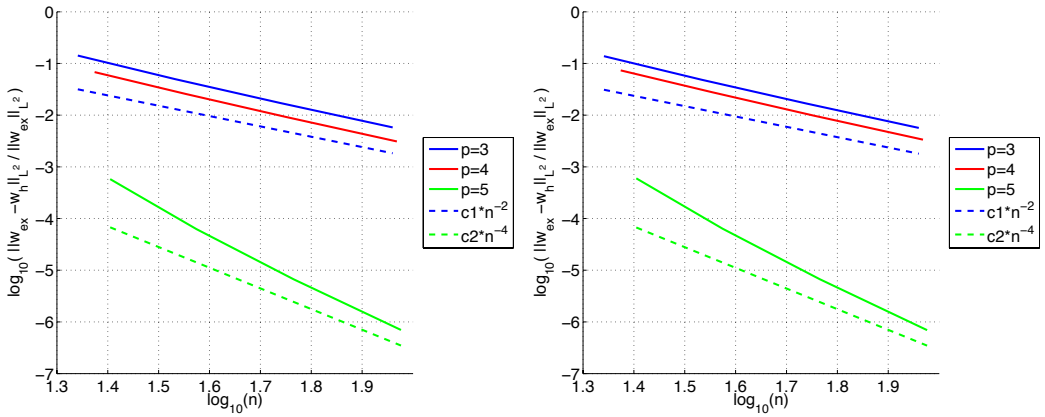

(a) $t = 10^{-1}$ (b) $t = 10^{-3}$

Fig. 3. Square plate with clamped support solved by a *primal formulation with rotated spaces*. L^2-norm approximation error of *displacement* for (a) a thick plate and (b) a thin plate.

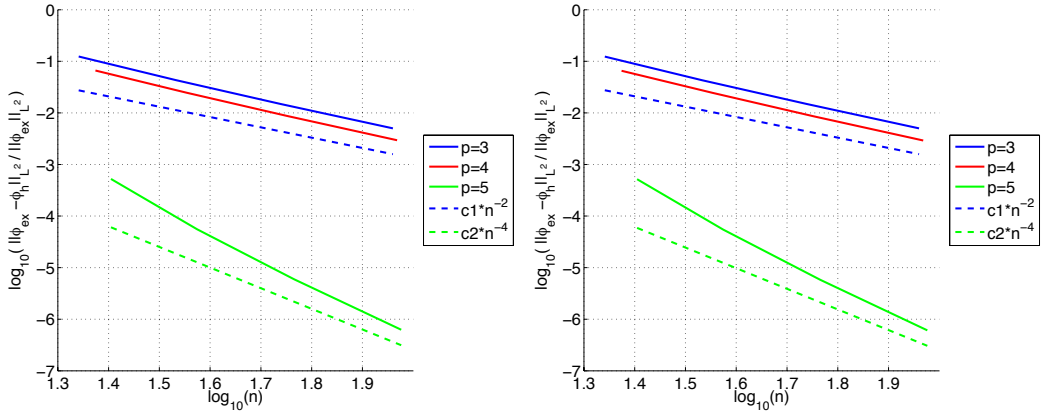

(a) $t = 10^{-1}$ (b) $t = 10^{-3}$

Fig. 4. Square plate with clamped support solved by a *primal formulation with rotated spaces*. L^2-norm approximation error of *rotations* for (a) a thick plate and (b) a thin plate.

The second example, consisting of a quarter annulus plate, includes non-linear geometrical mapping and different types of boundary conditions, and exhibits boundary layers.

5.1 Square plate with clamped support

We consider a problem for which an analytical solution is available (see [16]). This test consists of a unitary square plate $[0, 1]^2$ with clamped boundary conditions on all four sides and a distributed load given by the following

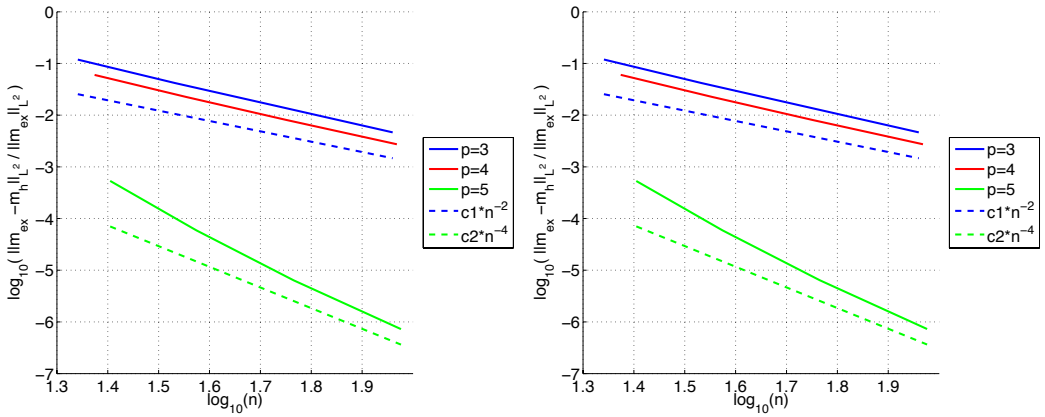

(a) $t = 10^{-1}$ (b) $t = 10^{-3}$

Fig. 5. Square plate with clamped support solved by a *primal formulation with rotated spaces*. L^2-norm approximation error of *bending moments* for (a) a thick plate and (b) a thin plate.

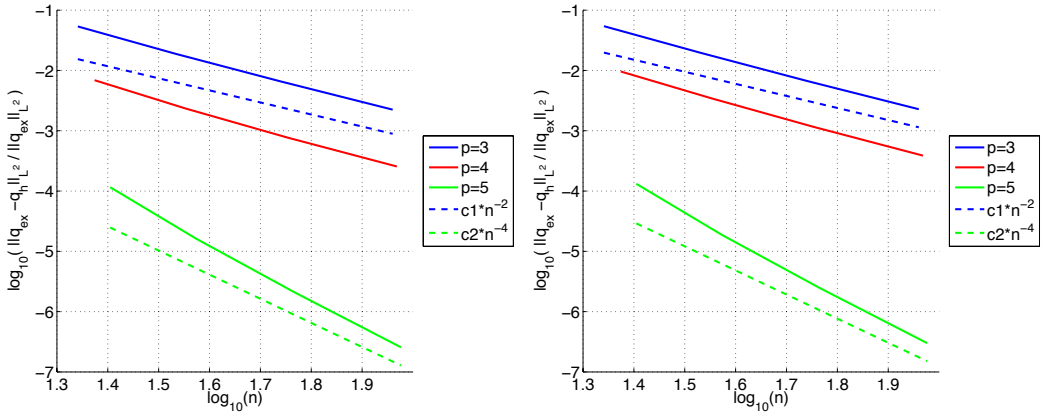

(a) $t = 10^{-1}$ (b) $t = 10^{-3}$

Fig. 6. Square plate with clamped support solved by a *primal formulation with rotated spaces*. L^2-norm approximation error of *shear forces* for (a) a thick plate and (b) a thin plate.

function:

$$
\begin{aligned}
f(x,y) = \frac{E}{12(1-\nu^2)}\big[&12y(y-1)(5x^2-5x+1)(2y^2(y-1)^2 \\
&+ x(x-1)(5y^2-5y+1)) \\
&+ 12x(x-1)(5y^2-5y+1)(2x^2(x-1)^2 \\
&+ y(y-1)(5x^2-5x+1))\big] \qquad (81)
\end{aligned}
$$

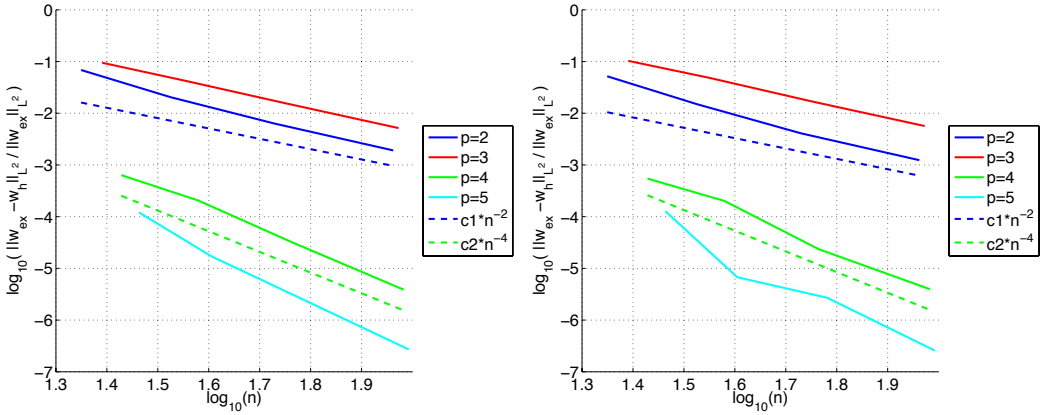

(a) $t = 10^{-1}$ (b) $t = 10^{-3}$

Fig. 7. Square plate with clamped support solved by a *mixed* formulation with equal orders. L^2-norm approximation error of *displacement* for (a) a thick plate and (b) a thin plate.

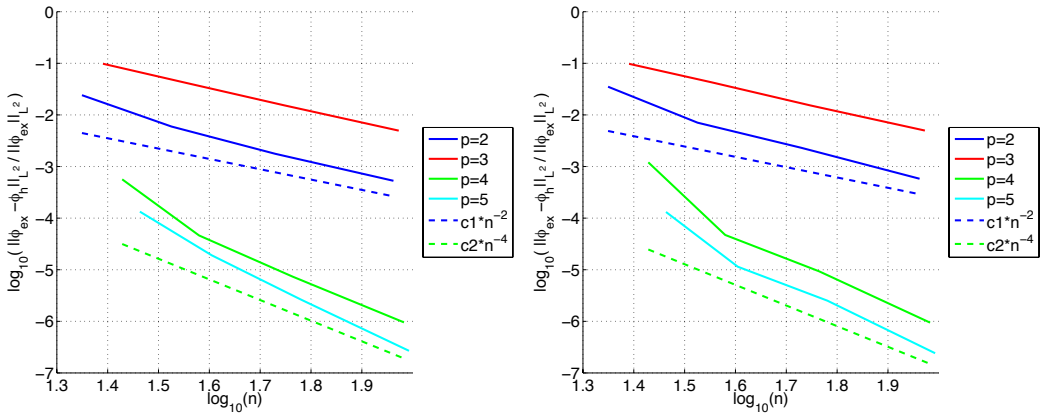

(a) $t = 10^{-1}$ (b) $t = 10^{-3}$

Fig. 8. Square plate with clamped support solved by a *mixed* formulation with equal orders. L^2-norm approximation error of *rotations* for (a) a thick plate and (b) a thin plate.

The analytical solution for displacement and rotations is given in [16] as:

$$\begin{aligned} w(x,y) = \frac{1}{3}x^3(x-1)^3y^3(y-1)^3 \\ - \frac{2t^2}{5(1-\nu)}\Big[y^3(y-1)^3x(x-1)(5x^2-5x+1) \\ + x^3(x-1)^3y(y-1)(5y^2-5y+1)\Big] \end{aligned} \tag{82}$$

$$\varphi_x(x,y) = -y^3(y-1)^3x^2(x-1)^2(2x-1) \tag{83}$$

$$\varphi_y(x,y) = -x^3(x-1)^3y^2(y-1)^2(2y-1) \tag{84}$$

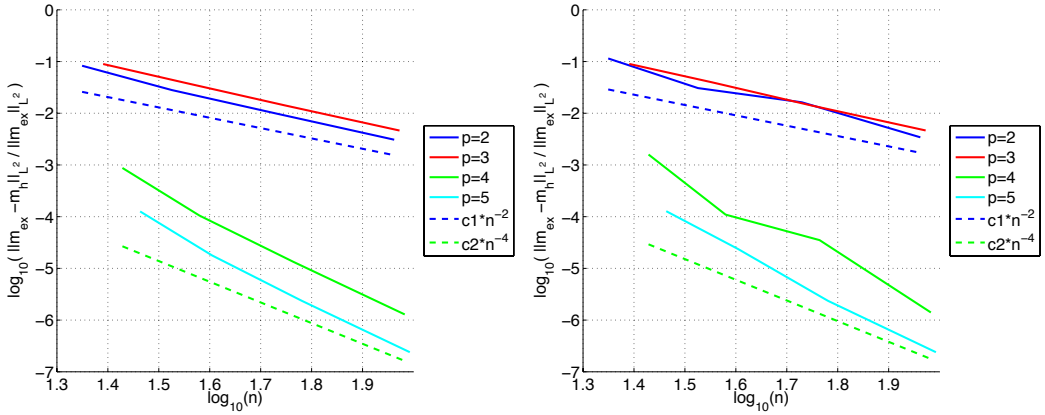

(a) $t = 10^{-1}$ (b) $t = 10^{-3}$

Fig. 9. Square plate with clamped support solved by a *mixed* formulation with equal orders. L^2-norm approximation error of *bending moments* for (a) a thick plate and (b) a thin plate.

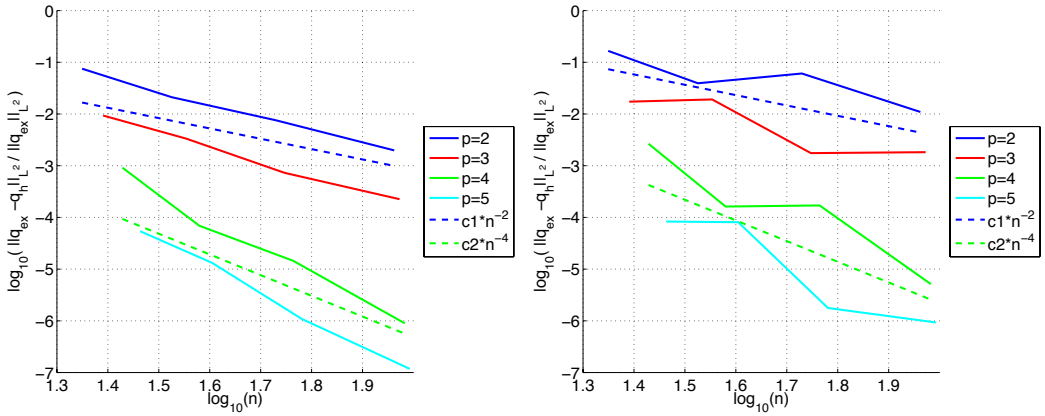

(a) $t = 10^{-1}$ (b) $t = 10^{-3}$

Fig. 10. Square plate with clamped support solved by a *mixed* formulation with equal orders. L^2-norm approximation error of *shear forces* for (a) a thick plate and (b) a thin plate.

From this, we also deduce the exact solution for bending moments and shear forces:

$$m_{xx} = -\frac{Et^3}{6(1-\nu^2)}\Big(y^3(y-1)^3(x-x^2)(5x^2-5x+1) + \nu(x^3(x-1)^3(y-y^2)(5y^2-5y+1))\Big) \tag{85}$$

$$m_{yy} = -\frac{Et^3}{6(1-\nu^2)}\Big(\nu(y^3(y-1)^3(x-x^2)(5x^2-5x+1)) + x^3(x-1)^3(y-y^2)(5y^2-5y+1)\Big) \tag{86}$$

$$m_{xy} = m_{yx} = -\frac{Et^3}{12(1+\nu)}3y^2(y-1)^2(2y-1)x^2(x-1)^2(2x-1) \tag{87}$$

$$q_x = -\frac{Et^3}{6(1-\nu^2)}\Big(y^3(y-1)^3(20x^3-30x^2+12x-1) + 3y(y-1)(5y^2-5y+1)x^2(x-1)^2(2x-1)\Big) \tag{88}$$

$$q_y = -\frac{Et^3}{6(1-\nu^2)}\Big(x^3(x-1)^3(20y^3-30y^2+12y-1) + 3x(x-1)(5x^2-5x+1)y^2(y-1)^2(2y-1)\Big) \tag{89}$$

The material parameters are given as $E = 10.92 \cdot 10^6$ and $\nu = 0.3$. In the following, the problem is solved by the proposed collocation methods, where for each study a thick plate with $t = 10^{-1}$ and a thin plate with $t = 10^{-3}$ are considered in order to investigate the presence of shear locking.

5.1.1 Primal formulation with equal orders

Firstly, we solve the problem by the primal collocation approach with equal orders, i.e., the same polynomial degree is used for displacement and rotations. A refinement study is performed for polynomial degrees $p = 2, 3, 4, 5$ and Figure 2 shows the L^2-norm approximation error of the displacement plotted against the square root of the total number of degrees of freedom $n = \sqrt{\#\text{dof}}$. Dashed lines indicate the order of convergence. As can be seen, the error converges well for all polynomial degrees in the case of a thick plate while shear locking is clearly present in the thin case. Regarding the thin plate, the results for $p = 4$ and $p = 5$ converge after some mesh refinement, while the results for $p = 2$ and $p = 3$ show no convergence at all in the range of considered meshes. Furthermore, it can be seen in Figure 2(a) that even degrees converge with a rate of p while odd degrees converge with $p - 1$. This characteristic *even-odd* switch in the convergence rates is typical for isogeometric collocation methods [3].

5.1.2 Primal formulation with rotated spaces

Secondly, the problem is solved by the primal approach with rotated spaces, as described in equations (47)-(53). The same refinement study as described above is performed. It is important to note that for the rotated spaces as described in (52)-(53) functions of degree $p - 1$ are involved, and, consequently, the minimum polynomial degree in this study is $p = 3$. Figure 3 shows the convergence of the L^2-norm approximation error of the displacement. As can be seen, the results converge well for both the thick and the thin plate, confirming that the primal formulation with rotated spaces is locking-free. Again, we can observe the characteristic *even-odd* switch, but now even degrees converge with $p - 1$ and odds with $p - 2$ due to the fact that analysis of degree p involves functions of degree $p - 1$. Additionally, we plot the convergence of the

L^2-norm approximation error of the rotations, bending moments, and shear forces, see Figure 4-6. Also these figures confirm the locking-free behavior of this method. Furthermore, it can be observed that displacement, rotations, bending moments, and shear forces are converging with the same convergence rates.

5.1.3 Mixed formulation with equal orders

Next, the mixed formulation with equal orders is employed to solve the problem and the results are displayed in Figures 7-10 depicting the error of displacement, rotations, bending moments, and shear forces. The results show that the mixed formulation is locking-free and that all variables converge with the same convergence rates.

5.1.4 Speed comparison

In this section, we want to compare the presented methods in terms of computational time effort. For the comparison, we measure the total time needed for assembly and solving of the plate problem presented above for the finest meshes and different polynomial degrees $p = 3, 4, 5$, comparing it for the approach with rotated spaces and the mixed formulation. The primal formulation with equal orders is not further considered here since it significantly suffers from locking. The mesh consists 50×50 elements for the primal formulation and 38×38 elements for the mixed formulation such that the total number of degrees of freedom is comparable. Additionally, we perform the same test with a corresponding Galerkin formulation, in particular, an isogeometric Galerkin formulation with equal orders using 50×50 elements as in the primal formulation. We remark that all methods have been programmed in Matlab using the same subroutines for shape functions etc., and all computations are run on a Laptop. We highlight that the following comparison serves just to give a speed estimate and surely is not to be considered as a precise measure of efficiency.

The results of the test are gathered in Table 1. As can be seen, the mixed formulation is significantly faster than the one with rotated spaces. This is because the mixed formulation requires only the evaluation of shape function derivatives, see (73)-(80), while the approach with rotated spaces requires additionally the Piola mapping of the rotations and their derivatives as described in equations (54)-(56). It is this additional mapping which makes the method with rotated spaces more costly in terms of computational time.

Moreover, it can be seen that both collocation methods are significantly faster than the Galerkin method especially for high polynomial degrees. We highlight again that this study is to be considered just as an estimate in terms of

computational time efficiency, comparing the methods for a certain size of the system matrix, without taking into account the absolute error obtained by the different methods. For a very detailed and comprehensive study on the efficiency of collocation methods based on error comparison, we refer to [33].

Method	$p = 3$	$p = 4$	$p = 5$
Collocation rotated spaces	15 s	17 s	18 s
Collocation mixed	5 s	6 s	7 s
Galerkin	37 s	56 s	93 s

Table 1
Computation time for assembly and solving of the quadratic plate example with different methods for the finest mesh and different polynomial degrees.

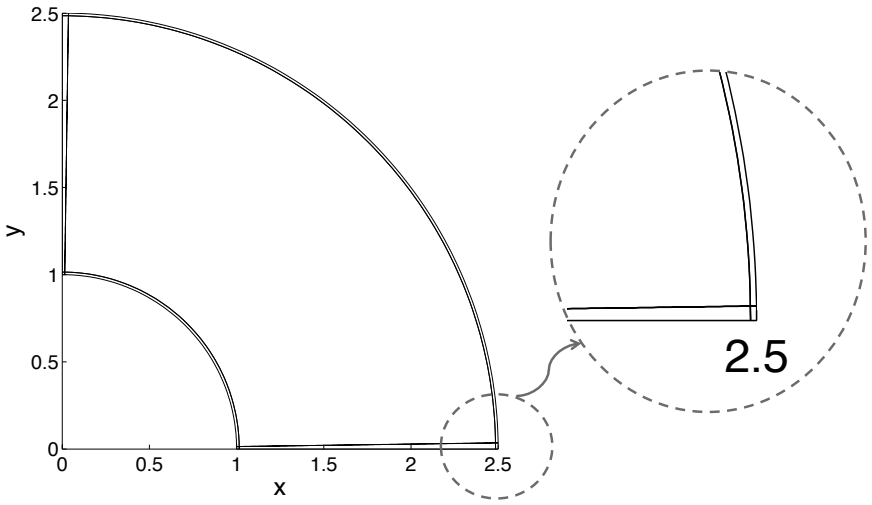

Fig. 11. Quarter annulus with boundary refinement on all four sides. The closeup shows a zoom of this refinement in the corner.

5.2 Quarter annulus

As a second example, we investigate the problem shown in Figure 11 representing a quarter of a circular annulus. The plate is subjected to a uniform load $f = 1$ and is simply supported at the straight edges while the curved

edges are free. The material and thickness parameters are $E = 10^8$, $\nu = 0.3$, and $t = 0.01$. As reported in [9], this problem exhibits boundary layers whose characteristic length is $O(t)$. In order to resolve these boundary layers, the following refinement scheme is employed. Given that the knot vectors of the initial model range from 0 to 1, a first refinement near the boundaries is performed by inserting knots at 0.01 and 0.99 in both directions, as shown in Figure 11. Based on this boundary-refined model, uniform refinement of the given knot spans is performed in the following. For solving the problem we

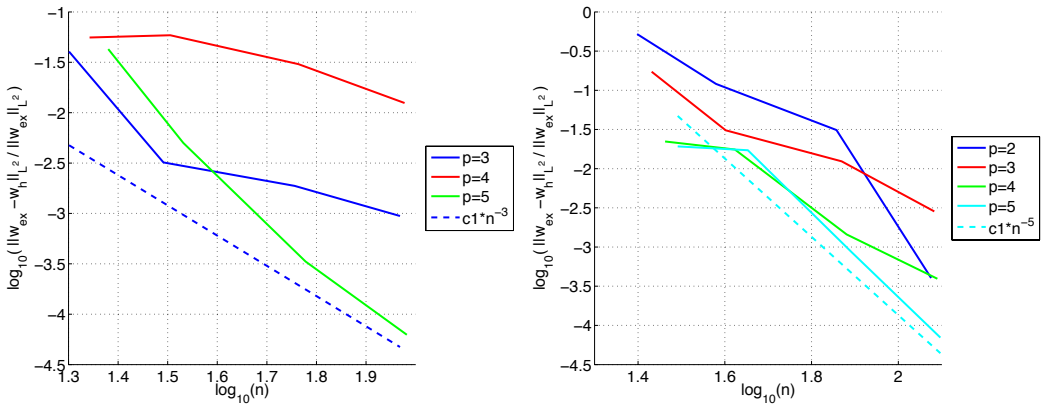

(a) (b)

Fig. 12. Quarter annulus with boundary refinement. L^2-norm approximation error of displacements using (a) the primal formulation with rotated spaces and (b) the mixed formulation with equal orders.

employ both the primal formulation with rotated spaces and the mixed formulation with equal orders. As in the previous example, convergence studies are made with polynomial degrees $p = 2, 3, 4, 5$ for the mixed formulation and $p = 3, 4, 5$ for the formulation with rotated spaces. Since no analytical solution is available for this example, the reference solution is computed on a very fine mesh with 120×120 quintic elements. Figure 12 shows the L^2-norm approximation error of the displacement for the two methods.

5.3 On the importance of compatible spaces and boundary layer resolution

In this section, we study the importance of two special aspects of the presented methods, in particular, the use of compatible spaces, i.e., rotated spaces with Piola mapping in case of a primal formulation, and boundary refinement in case of boundary layers. It is noted that these techniques are also necessary in corresponding Galerkin formulations [9] in order to obtain optimal convergence. However, it appears that their correct application is much more significant in collocation methods. In order to demonstrate these effects, we repeat the annulus example, once without boundary refinement and once without compatible spaces for the primal formulation.

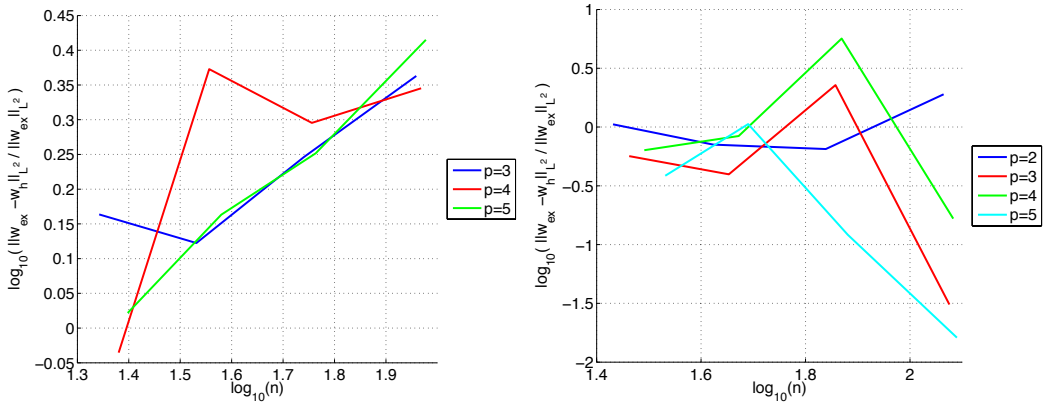

(a) (b)

Fig. 13. Quarter annulus *without* boundary refinement. L^2-norm approximation error of displacements using (a) the primal formulation with rotated spaces and (b) the mixed formulation with equal orders.

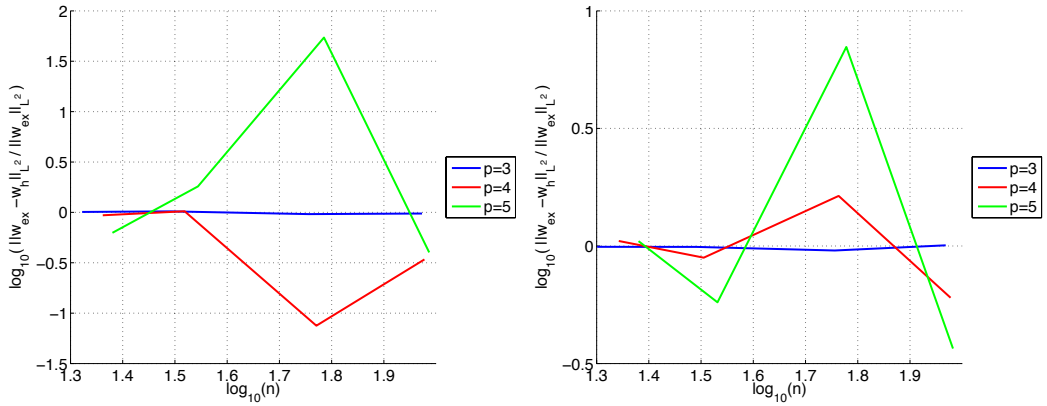

(a) (b)

Fig. 14. Quarter annulus with boundary refinement. L^2-norm approximation error of displacements using a primal formulation (a) with equal orders and (b) with rotated spaces but without Piola mapping.

Firstly, we rerun the annulus example with the same formulations as before, but without the proposed boundary refinement. The results are depicted in Figure 13. As can be seen, the results of the primal formulation are diverging, and also for the mixed formulation convergence is obtained only for $p > 2$ and after some refinement. This behavior is quite different from corresponding Galerkin formulations where not resolving the boundary layers just leads to lower convergence rates, see [9].

Furthermore, we solve the same example performing boundary refinement as described above but using the primal formulation with equal orders. While in the example of a square plate with clamped boundaries typical locking behavior was observed, i.e., the plate behaves "too stiff" for lower orders, cf. Figure 2(a), the behavior is quite different in this example and cannot be clas-

sified as a typical locking problem. As can be seen in Figure 14(a), the results look rather "chaotic" and the L^2-norm error takes on values larger than one. Plotting the deformation of the plate we have observed even negative deformations, i.e., deformations in the opposite direction of the loading. Similar results are also obtained if rotated spaces are used for discretizing $\varphi_\xi, \varphi_\eta$ but without the correct Piola mapping as described in (54)-(56), see Figure 14(b).

As a conclusion from these tests, one can observe that the presented collocation methods exhibit problems in the same cases as corresponding Galerkin formulations, but the negative effects are more severe. The reason for such behavior is not completely understood yet and will be subject of further research. Nevertheless, the methods work well if compatible spaces (or a mixed formulation) are used and boundary layers are properly resolved as proposed in this paper.

6 Conclusions

In the present paper, we have introduced isogeometric collocation schemes for the approximation of Reissner-Mindlin plates. Both primal (i.e., based on displacements and rotations) and mixed (i.e., based on displacements, rotations, and shear forces) formulations have been studied. In particular, we have considered a primal formulation based on equal order approximations, a primal formulation based on "rotated" (compatible) spaces complemented by a suitable Piola mapping, and a mixed formulation based on equal order approximations. Such formulations have been carefully tested in different geometric and boundary condition situations. Moreover, their performance in the thin limit has been tested as well, and, in particular, it has been shown that the primal formulation based on rotated spaces and the equal order mixed formulation appear to be free of shear locking. The numerical tests have shown that the use of compatible spaces and the correct resolution of boundary layers is even more important than in corresponding Galerkin formulations, a fact, which will be subject to further investigations in future research. Also, some preliminary comparisons in terms of computational time have been presented, giving indications about the efficiency of isogeometric collocation.

Possible interesting lines of future research include the extension of the presented formulations to the nonlinear regime, as well as to the approximation of shell structures.

Acknowledgments

The authors were partially supported by the European Research Council through the FP7 Ideas Starting Grant n. 259229 *ISOBIO*, by the European Commission through the FP7 Factory of the Future project *TERRIFIC* (FoF-ICT-2011.7.4, Reference: 284981), as well as by the Italian MIUR through the FIRB "Futuro in Ricerca" Grant RBFR08CZ0S. These supports are gratefully acknowledged.

References

[1] D. N. Arnold and R. S. Falk. Asymptotic Analysis of the boundary layer for the Reissner-Mindlin plate model. *SIAM Journal on Mathematical Analysis*, 27:486–514, 1996.

[2] F. Auricchio, L. Beirão da Veiga, A. Buffa, C. Lovadina, A. Reali, and G. Sangalli. A fully "locking-free" isogeometric approach for plane linear elasticity problems: A stream function formulation. *Computer Methods in Applied Mechanics and Engineering*, 197:160–172, 2007.

[3] F. Auricchio, L. Beirão da Veiga, T.J.R. Hughes, A. Reali, and G. Sangalli. Isogeometric collocation methods. *Mathematical Models and Methods in Applied Sciences*, 20(11):2075–2107, 2010.

[4] F. Auricchio, L. Beirão da Veiga, T.J.R. Hughes, A. Reali, and G. Sangalli. Isogeometric collocation for elastostatics and explicit dynamics. *Computer Methods in Applied Mechanics and Engineering*, 249-252:2–14, 2012.

[5] F. Auricchio, L. Beirão da Veiga, J. Kiendl, C. Lovadina, and A. Reali. Locking-free isogeometric collocation methods for spatial Timoshenko rods. *Computer Methods in Applied Mechanics and Engineering*, 263:113–126, 2013.

[6] F. Auricchio, F. Calabrò, T.J.R. Hughes, A. Reali, and G. Sangalli. A simple algorithm for obtaining nearly optimal quadrature rules for NURBS-based isogeometric analysis. *Computer Methods in Applied Mechanics and Engineering*, 249–252:15–27, 2012.

[7] K.-J. Bathe. *Finite Element Procedures*. Prentice-Hall, Berlin, 1996.

[8] Y. Bazilevs, L. Beirão da Veiga, J.A. Cottrell, T.J.R. Hughes, and G. Sangalli. Isogeometric analysis: approximation, stability and error estimates for h-refined meshes. *Mathematical Models and Methods in Applied Sciences*, 16:1–60, 2006.

[9] L. Beirão da Veiga, A. Buffa, C. Lovadina, M. Martinelli, and G. Sangalli. An isogeometric method for the Reissner-Mindlin plate bending problem. *Computer Methods in Applied Mechanics and Engineering*, 209-212:45–53, 2012.

[10] L. Beirão da Veiga, A. Buffa, J. Rivas, and G. Sangalli. Some estimates for $h-p-k-$refinement in isogeometric analysis. *Numerische Mathematik*, 118:271–305, 2011.

[11] L. Beirão da Veiga, T.J.R. Hughes, J. Kiendl, C. Lovadina, J. Niiranen, A. Reali, and H. Speelers. A locking-free model for Reissner-Mindlin plates: Analysis and isogeometric implementation via NURBS and triangular NURPS. *In preparation*, 2014.

[12] L. Beirão da Veiga, C. Lovadina, and A. Reali. Avoiding shear locking for the Timoshenko beam problem via isogeometric collocation methods. *Computer Methods in Applied Mechanics and Engineering*, 241-244:38–51, 2012.

[13] D. Boffi, F. Brezzi, and M. Fortin. *Mixed Finite Element Methods and Applications*. Springer-Verlag, Berlin, 2013.

[14] A. Buffa, J. Rivas, G. Sangalli, and R. Vázquez. Isogeometric discrete differential forms in three dimensions. *SIAM Journal of Numerical Analysis*, 49:818–844, 2011.

[15] A. Buffa, G. Sangalli, and R. Vázquez. Isogeometric analysis in electromagnetics: B-splines approximation. *Computer Methods in Applied Mechanics and Engineering*, 199:1143–1152, 2010.

[16] C. Chinosi and C. Lovadina. Numerical analysis of some mixed finite element methods for Reissner-Mindlin plates. *Computational Mechanics*, 16:36–44, April 1995.

[17] J.A. Cottrell, T.J.R. Hughes, and Y. Bazilevs. *Isogeometric Analysis: Toward Integration of CAD and FEA*. Wiley, 2009.

[18] J.A. Cottrell, A. Reali, Y. Bazilevs, and T.J.R. Hughes. Isogeometric analysis of structural vibrations. *Computer Methods in Applied Mechanics and Engineering*, 195:5257–5296, 2006.

[19] L. De Lorenzis, J.A. Evans, T.J.R. Hughes, and A. Reali. Isogeometric collocation: Neumann boundary conditions and contact. *Computer Methods in Applied Mechanics and Engineering*, doi:10.1016/j.cma.2014.06.037, 2014.

[20] R. Echter, B. Oesterle, and M. Bischoff. A hierarchic family of isogeometric shell finite elements. *Computer Methods in Applied Mechanics and Engineering*, 254(0):170 – 180, 2013.

[21] H. Gomez, V. M. Calo, Y. Bazilevs, and T. J. R. Hughes. Isogeometric analysis of the Cahn–Hilliard phase-field model. *Computer Methods in Applied Mechanics and Engineering*, 197:4333–4352, 2008.

[22] H. Gomez, A. Reali, and G. Sangalli. Accurate, efficient, and (iso)geometrically flexible collocation methods for phase-field models. *Journal for Computational Physics*, 262:153–171, 2014.

[23] T.J.R. Hughes. *The Finite Element Method, Linear Static and Dynamic Finite Element Analysis*. Dover Publications Inc., 2000.

[24] T.J.R. Hughes, J.A. Cottrell, and Y. Bazilevs. Isogeometric analysis: CAD, finite elements, NURBS, exact geometry, and mesh refinement. *Computer Methods in Applied Mechanics and Engineering*, 194:4135–4195, 2005.

[25] T.J.R. Hughes, A. Reali, and G. Sangalli. Duality and unified analysis of discrete approximations in structural dynamics and wave propagation: Comparison of p-method finite elements with k-method NURBS. *Computer Methods in Applied Mechanics and Engineering*, 197:4104–4124, 2008.

[26] T.J.R. Hughes, A. Reali, and G. Sangalli. Efficient quadrature for NURBS-based isogeometric analysis. *Computer Methods in Applied Mechanics and Engineering*, 199:301–313, 2010.

[27] T.J.R Hughes and T.E. Tezduyar. Finite elements based upon Mindlin plate theory with particular reference to the four-node bilinear isoparametric element. *Journal of Applied Mechanics*, 48:587–596, 1981.

[28] J. Kiendl, K.-U. Bletzinger, J. Linhard, and R. Wüchner. Isogeometric shell analysis with Kirchhoff-Love elements. *Computer Methods in Applied Mechanics and Engineering*, 198:3902–3914, 2009.

[29] Q. Long, P.B. Bornemann, and F. Cirak. Shear-flexible subdivision shells. *International Journal for Numerical Methods in Engineering*, 90(13):1549–1577, 2012.

[30] S. Morganti, F. Auricchio, D.J. Benson, F.I. Gambarin, S. Hartmann, T.J.R. Hughes, and A. Reali. Patient-specific isogeometric structural analysis of aortic valve closure. *ICES Report*, 14-10, 2014.

[31] A. Reali. An isogeometric analysis approach for the study of structural vibrations. *Computer Methods in Applied Mechanics and Engineering*, 1–30:15–27, 2006.

[32] A. Reali and H. Gomez. An isogeometric collocation approach for Bernoulli-Euler beams and Kirchhoff plates. *Submitted*, 2014.

[33] D. Schillinger, J.A. Evans, A. Reali, M.A. Scott, and T.J.R. Hughes. Isogeometric collocation: Cost comparison with Galerkin methods and extension to adaptive hierarchical NURBS discretizations. *Computer Methods in Applied Mechanics and Engineering*, 267:170–232, 2013.

[34] D. Schillinger, S.J. Hossain, and T.J.R. Hughes. Reduced Bézier element quadrature rules for quadratic and cubic splines in isogeometric analysis. *Computer Methods in Applied Mechanics and Engineering*, 277:1–45, 2014.

[35] S. Shojaee, E. Izadpanah, N. Valizadeh, and J. Kiendl. Free vibration analysis of thin plates by using a NURBS-based isogeometric approach. *Finite Elements in Analysis and Design*, 61:23–34, 2012.